(Received 18 February 2025, Accepted 1 April 2025, Scheduled 9 April 2025)

Design of a Triple-Band Metamaterial Bandpass Filter Utilizing Modified-Minkowski Fractal Geometry

Hayder S. Ahmed* and Aqiel N. Almamori

Electronic and Communications Department, College of Engineering, University of Baghdad, Iraq

ABSTRACT: In this paper, a triple-band bandpass filter based on metamaterials and fractal geometry is proposed. The proposed filter is designed based on three concepts. First, Transmission Lines (TLs) function both as feed lines and as resonators at high frequencies. Second, metamaterials open loop 0th iteration Modified-Minkowski resonators are employed for the middle-frequency band. Third, at a lower frequency, in the 1st iteration, Modified-Minkowski resonators are introduced in the space between TLs to optimize space utilization. The proposed filter has been designed at center frequencies 11 GHz, 6 GHz, and 5 GHz by using a Rogers RO 4003 substrate with a thickness of 1.5 mm and dielectric constant of 3.5, resulting in an overall size of 32.2 mm $\times$ 20.6 mm. The design simulation is performed using CST microwave studio. To validate the results, the proposed filter has been fabricated. A strong correlation between the measured and simulated results confirms the effectiveness of the design. The proposed filter has three bands at 5 GHz, 6 GHz, and 11 GHz with corresponding S_{21} values of -0.39 dB, -1 dB, and -0.26 dB and a size reduction of 31% compared with conventional Dual-Band Bandpass Filter for wireless applications.

1. INTRODUCTION

Over the past 50 years, communication systems have rapidly evolved. One of the biggest challenges that manufacturers face has been the large size of these systems. To address this, researchers have focused on miniaturization techniques. One such approach involves designing multiband structures, enabling multiple applications within a single compact device [1–10]. Several studies [1–4, 10, 11] have explored the design of single and multi-band bandpass filters (BPFs), while multi-band band-stop filters (BSFs) have been investigated in [5, 6]. Additionally, dual-band antennas have also been a key area of interest [7–9].

Another effective miniaturization technique involves using fractal geometries. Various fractal structures, such as Peano, Minkowski, Koch, and meander line configurations, have been utilized to achieve size reduction [4–6, 12–16]. This technique is highly effective in maintaining the center frequency while significantly reducing the overall structure size. The concept relies on filling available space, thereby increasing the current distribution path and enhancing miniaturization.

A novel dual-band bandpass microstrip filter (DBBPF) is introduced and explored for RF/microwave applications. The design methodology incorporates two primary principles: first, the implementation of metamaterial resonators in the form of C-shaped split rings (C-SRRs) to achieve left-handed (LH) behavior while minimizing losses, and second, the integration of a microstrip feed line that is folded ensures compactness [1]. Another approach to dual-band bandpass filter design is presented in [2], where a hybrid resonator structure derived from a microstrip patch is employed. In this design, rectangular microstrip rings excite the TE200 and TE002 modes of a patch resonator, forming a high-frequency passband, while simultaneously functioning as a resonator to create the low-frequency passband.

A compact dual-band bandpass filter is developed, investigated, and fabricated in [3]. This design features a loop resonator combined with two modified T-shaped resonators, dual T-shaped resonators, and open-bended stubs to achieve dual-band operation. Another method for miniaturization employs a fractal geometry, as demonstrated in [4], where a multiband microstrip bandpass filter is designed based on a fractal open-loop structure. The filter consists of an array of equal-sided open-loop resonators, each exhibiting a different level of fractal iteration.

For band-stop filter (BSF) applications, Peano fractal-based open-loop resonators were adopted in developing dual-band microstrip BSFs. This design is based on conventional rectangular open-loop microstrip resonators, modified by using Peano fractal geometry with varying iteration degrees [5]. The band-stop functionality at lower frequencies is associated with resonators having higher iteration levels, while the band-stop performance at higher frequencies is due to resonators with lower iteration levels. A triple-band BSF leveraging Minkowski fractal geometry has also been developed, with various structures evaluated using a commercial electromagnetic (EM) simulation tool [6].

A compact dual-band rectangular microstrip antenna (RMSA) is developed by integrating two single-band rectangular microstrip antennas, each incorporating a single slot and an altered ground plane. The introduction of open-ended slots

* Corresponding author: Hayder S. Ahmed (hayder.s@coeng.uobaghdad.edu.iq).

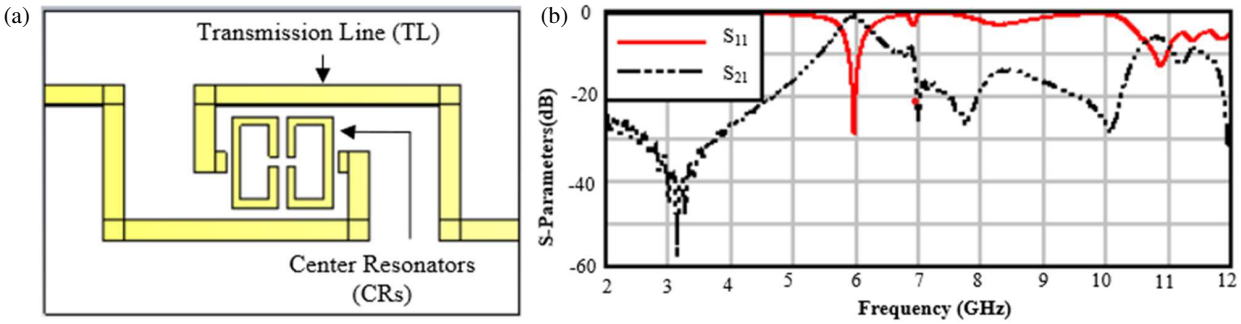

FIGURE 1. (a) The traditional DB-BPF [1]. (b) S_{11} and S_{21} of conventional DB-BPF.

in each antenna generates wide impedance bandwidths, which shift to lower frequencies due to ground slot effects [7]. In another design, a microstrip patch antenna operating at 2.4 GHz and 5.8 GHz is developed for Wi-Fi applications. This antenna consists of a patch conductor with three slots and an FR-4 substrate underneath [8]. A similar approach is taken in [9], where a dual-band rectangular microstrip patch antenna with a defected ground structure is designed for operation at 2.5 GHz and 3.5 GHz. Here, two slots are etched into the ground plane of a patch antenna originally designed for 2.5 GHz operation, thereby enabling the second frequency band at 3.5 GHz.

Several fractal geometries have been explored for miniaturization in various designs. In [12], a combination of the dual-mode technique and a fractal-based resonator is employed to create a compact band-reject filter. This design utilizes triangular patch resonators with embedded slits, while the Koch fractal geometry is applied to the uncoupled edges of the triangular patch. Another fractal-based dual-mode microstrip BSF is introduced in [13], where Minkowski fractal geometry is integrated into a conventional triangular dual-mode resonator to achieve a more compact structure with enhanced selectivity.

A further reduction in size is achieved through the use of meander-line resonators. A miniaturized microstrip band-pass filter is demonstrated in [14], featuring a meander-line resonator with significantly reduced dimensions, approximately $\lambda_g/8 \times \lambda_g/8$ at a center frequency of 2.445 GHz. Additionally, a compact low-pass filter based on an N-turn meander-line structure is proposed in [15]. This low-pass filter exhibits a transmission zero near the passband edge and maintains low insertion loss within the passband. The filter's cutoff frequency and transmission zero position can be controlled by adjusting the dimensions of the meander line, making it a versatile design. A comprehensive study on band-reject filter techniques is provided in [16], showcasing various methods for reducing microwave radiation. The book introduces a novel compact fractal band-reject filter, specifically designed at 2.45 GHz to mitigate microwave oven leakage, thereby enhancing electromagnetic compatibility and reducing interference.

In this paper, a Triple-Band Band-Pass Filter (TBPF) is designed with center frequencies of 5 GHz, 6 GHz, and 11 GHz for RF/microwave applications. The design is based on two key concepts: metamaterial resonators, incorporating the 0th and 1st iterations of a modified Minkowski fractal geometry, and a transmission line, which serves both as a feed and an additional resonator. The filter is fabricated using a Rogers RO4003 substrate with a thickness of 1.5 mm and a dielectric constant of 3.5. The design is simulated using Computer Simulation Technology (CST) software. To verify its performance, the filter was fabricated, and the measured results show good agreement with the simulation.

2. ANALYSIS OF CONVENTIONAL DUAL-BAND BPF

The conventional Dual-Band Band-Pass Filter (DB-BPF), shown in Fig. 1(a), is designed based on two key concepts using a Rogers RO4003 substrate with a thickness of 1.5 mm and a dielectric constant of 3.5. The feeding transmission line has a width (W_L) of 1.4 mm and a characteristic impedance (Z_0) of 80 Ω, calculated using the equations in [17].

$$\epsilon_e = \frac{\epsilon_r + 1}{2} + \frac{\epsilon_r - 1}{2} \frac{1}{\sqrt{1 + 12h/W_L}} \tag{1}$$

$$Z_0 = \begin{cases} \frac{60}{\sqrt{\epsilon_e}} \ln\left(\frac{8h}{W_L} + \frac{W_L}{4h}\right) & for\ W_L/h \leq 1 \\ \frac{120\pi}{\sqrt{\epsilon_e}[W_L/h + 1.393 + 0.667\ln(W_L/h + 1.444)]} & for\ W_L/h \geq 1 \end{cases} \tag{2}$$

The structure was re-simulated using CST, based on the dimensions provided in [1]. As shown in Fig. 1(b), the filter exhibits two frequency bands:

- The first band appears at 11.9 GHz, with $S_{11} = -12.27$ dB and $S_{21} = -6$ dB at the center frequency.
- The second band is at 5.9 GHz, with $S_{11} = -28.26$ dB and $S_{21} = -1$ dB.

There are minor variations in S_{11} and S_{21} compared to [1], which are attributed to slight differences in proximity dimensions, as illustrated in Fig. 1(b).

The structure consists of two main components:

1. Transmission Lines (TLs)
2. Center Resonators (CRs) (Fig. 1(a))

The transmission lines serve as feeds for the center resonators, generating the first mode at 10.9 GHz. As shown in Fig. 2(a), the E-field distribution is concentrated on the TLs at 10.9 GHz.

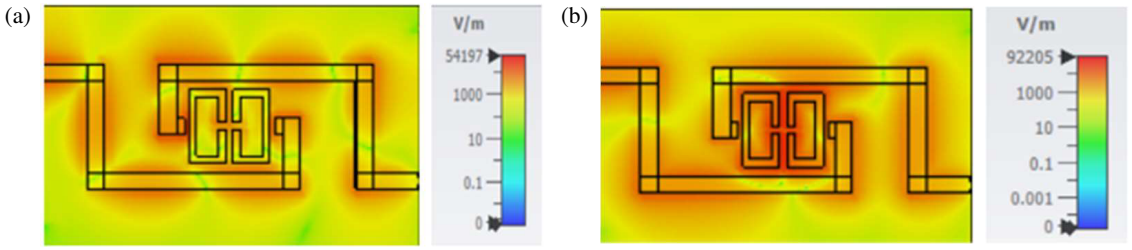

FIGURE 2. (a) E-filed distribution at 10.9 GHz. (b) E-filed distribution at 5.9 GHz .

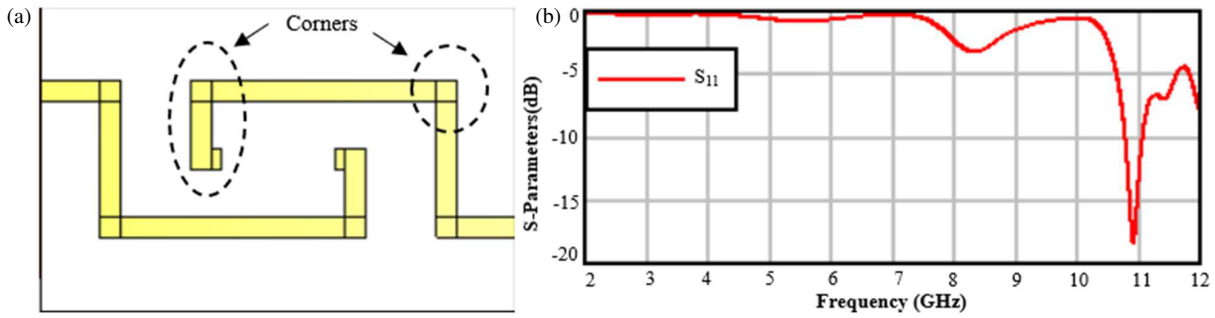

FIGURE 3. (a) Conventional BPF with TLs only. (b) S_{11} of Conventional BPF with TLs only .

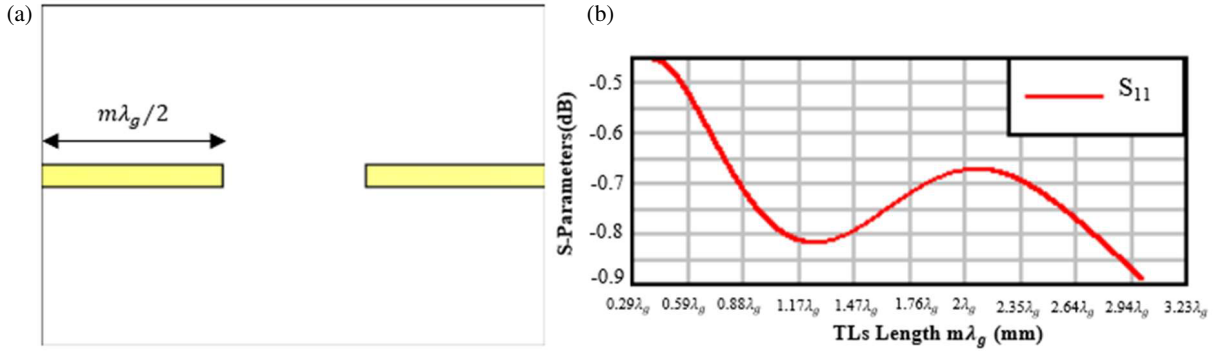

FIGURE 4. (a) The structure with straight TLs. (b) S_{11} of different lengths of $m\lambda_g/2$ at 10.9 GHz.

The center resonators are C-shape resonators that are constructed to produce the second mode and have a metamaterials property.

The length of TLs equals $2.5\lambda_g$, where λ_g is the guided wavelength that can be calculated by:

$$\lambda_g = \frac{\lambda_o}{\sqrt{\epsilon_e}} \tag{3}$$

and

$$\lambda_o = \frac{c}{f} \tag{4}$$

where λ_0 is the free space wavelength, ϵ_e the effective permittivity, f the center frequency, and c the light speed. To confirm the role of the transmission lines (TLs), the structure was simulated with only TLs, as shown in Fig. 3. The results in Fig. 3(b) indicate that only one resonance appears at 10.9 GHz, while the second resonance is eliminated. The S_{11} value at 10.9 GHz is -17.9 dB, confirming that the TLs are responsible for generating the first mode.

Most researchers use $0.5\lambda_g$ to achieve resonance with compact structures, allowing multiple segments of $0.5\lambda_g$ to produce the same resonance effect. To verify this principle, the authors simulate structures with straight transmission lines of different lengths ($m\lambda_g/2$) using CST microwave studio, as shown in Fig. 4(a).

From Fig. 4(b), the S_{11} values at 10.9 GHz for different lengths of straight transmission lines (TLs) range between -0.45 dB and -0.9 dB. This indicates that resonance does not occur at 10.9 GHz with either $0.5\lambda_g$ or $2.5\lambda_g$ straight TLs, which have the same length as the TLs in the conventional structure. As a result, these straight TLs cannot be used to generate the mode at 10.9 GHz.

In contrast, the curved structure of the conventional design, which includes three corners with TLs, minimizes characteristic impedance and reflection losses, allowing resonance to occur at 10.9 GHz, as shown in Fig. 3 [18].

The second part of the conventional structure consists of center resonators (CRs), which are open-loop resonators, as

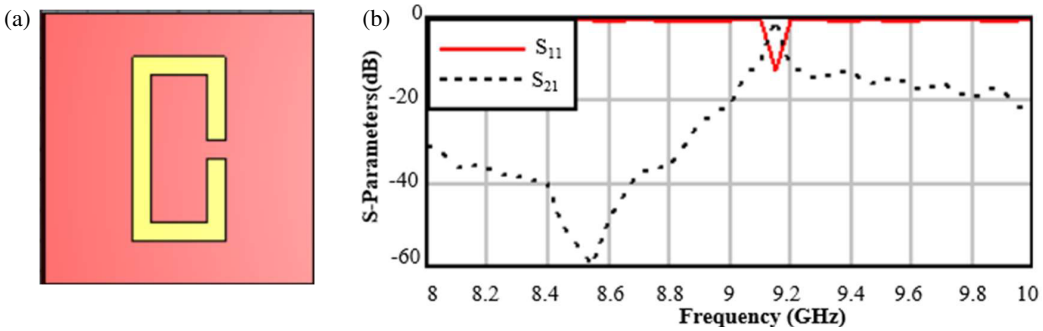

FIGURE 5. (a) CRS unit cell. (b) S-parameters of it.

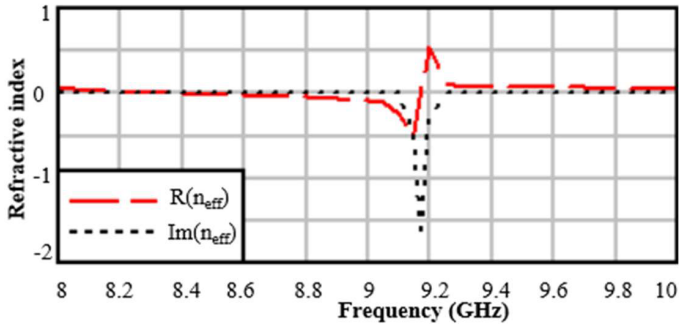

FIGURE 6. Extracted real part and imaginary part of Refractive index of the CRs.

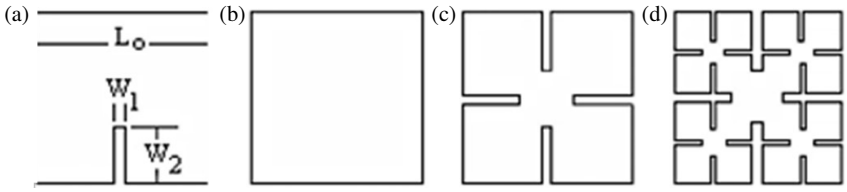

FIGURE 7. The Minkowski fractal geometry: (a) the generator, (b), (c), and (d) represent the 0th, 1st, and 2nd iteration levels, respectively [4] and [6].

shown in Fig. 1(a). According to [1], these resonators exhibit metamaterial properties. The unit cell has been re-stimulated by using CST with a Rogers RO 4003 substrate of thickness $h = 1.5$ mm and dielectric constant equal to 3.5, with overall size 8.8 mm × 8.8 mm as shown in Fig. 5 with S-parameters.

The effective parameters of the CRs are extracted by using the Nicolson-Ross-Weir (NRW) method [19, 20], and the refractive index of the C-SRR (Split Ring Resonator) is given by Eq. (5) [21].

$$n_{eff} = \frac{c}{j\pi fh} \times \sqrt{\left[\frac{1-(S_{21}+S_{11})}{1+(S_{21}+S_{11})}\right]\left[\frac{1-(S_{21}-S_{11})}{1+(S_{21}-S_{11})}\right]} \quad (5)$$

From the imaginary and real parts of the refractive index shown in Fig. 6, the CRs have negative values (simultaneously) in the frequency range around the resonance of 9.17 GHz. This characteristic can justify the left-handed (LH) electromagnetic behavior of the proposed metamaterial resonator.

Figure 2(b) presents the E-field distribution at 5.9 GHz, where the E-field is concentrated on the CRs, indicating that they generate the second mode. The length of each resonator is $0.5\lambda_g$.

3. METHODOLOGY

Fractal geometry is used to design a triple-band filter with the same size as the dual-band filter proposed by [1] by adding different resonator iterations. Modified-Minkowski fractal geometry with added iterations is applied to an open-loop rectangle resonator.

The common Modified-Minkowski geometries with different iterations, 0th [4–6], 1st, and 2nd, are shown in Fig. 7, respectively.

The perimeter P_n of the nth iteration is given by [4] and [6]

$$P_n = \left(1 + \frac{2w_2}{L_o}\right) P_{n-1} \quad (6)$$

where w_2 and L_o are as shown in Fig. 5. Eq. (6) implies that, as n approaches infinity, the perimeter goes to infinity.

The objective of using fractal geometry is to increase the surface current path length. Consequently, for a given design frequency, it enables either a reduced resonant frequency or a smaller resonator size [4] and [6].

Figure 8 illustrates the application of the Modify-Minkowski technique to rectangular open-loop resonators at both the 0th

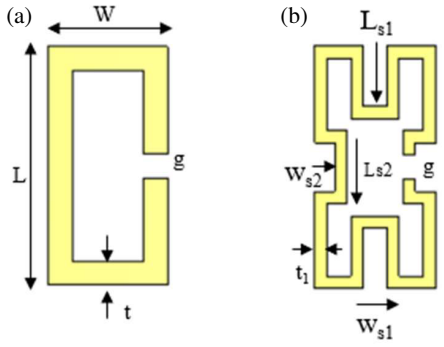

FIGURE 8. (a) Rectangle open loop resonator with 0th iteration. (b) Rectangle open loop resonator with Modify-Minkowski 1st iteration.

and first iterations. The outer dimensions of these resonators remain consistent at $L \times W$ for both iterations. Consequently, this study utilizes two rectangular open-loop resonators — one at 0th iteration and the other at the first iteration — with identical outer dimensions to achieve dual-band operation.

The perimeter P_n of the nth iteration of rectangle resonators without the gap "g" is given by

$$P_n = \left(1 + \frac{2L_{s1}}{W} + \frac{2w_{s2}}{L}\right) P_{n-1} \tag{7}$$

where W, w_{s1}, L, and L_{s1} are as shown in Fig. 8. Eq. (7) implies that, as n approaches infinity, the perimeter goes to infinity. The perimeter of open loop rectangle with Modify-Minkowski resonator for the nth iteration is given by:

$$L_n = p_n - g \tag{8}$$

4. PROPOSED TRIPLE-BANDS BPF DESIGN

The design of the proposed BPF starts from the conventional structure that shown in Fig. 1(a), which consists of two TLs and two open loop metamaterials resonators that represent the 0th iteration Modify-Minkowski resonators also. In addition, the authors add two resonators after applying the 1st iteration Modify-Minkowski in the spaces between TLs to use the spaces with length approximately equal to $0.6\lambda_g$ to get the third band at 5 GHz. A Rogers RO 4003 substrate with thickness $h = 1.5$ mm and dielectric constant equal to 3.5 has been used to design the BPF. The overall size of the proposed BPF is 32.2 mm $\times$ 20.6 mm. To simulate the proposed BPF, CST has been used as shown in Fig. 9 with flat copper ground plane. The feeding transmission line width (W_L) was 1.4 mm with characteristic impedance (Z_0) equal to 80 Ω. However, the authors consider the waveguide port constant to get match with input and output impedance 50 Ω that simulate the practical case. Here, the mismatch between the TLs and input and output port is expected. All the dimensions of the proposed structure are listed in Table 1. From Fig. 9(c). the third band at 5 GHz does not appear, while the second band at 6 GHz has a critical S_{11} that was -11 dB with -1 dB S_{21}. In contrast, the first band at 10.9 GHz shifts to 11.27 GHz with S_{11} equal to -18 dB, but the S_{21} becomes better than the conventional BPF and reaches -1.79 dB. Fig. 9(c) shows that the added open loop of the 1st iteration resonators improves the S_{21} and impedance matching between the TLs and ports. The authors study parameter D, which is the gap between the TL and open loop 1st iteration resonator as shown in Fig. 9(a) with a range from 0.9 mm to 0.1 mm to increase the coupling between the TLs and resonators. CST is used to find the optimized value of D as shown in Fig. 10.

TABLE 1. The dimensions of the proposed BPF.

Parameters	Value (mm)	Parameters	Value (mm)
Width	32.2	Length	20.6
W_L	1.4	D	0.9
L_{F1}	5.4	L_{F2}	9.2
L_{F3}	18	L_{F4}	6
Lg	7.6	z	0.61
L	6.24	W	3.12
g	0.624	t	0.624
L_{s1}	1.5	L_{s2}	1.8
W_{s1}	0.6	W_{s2}	0.5
t_1	0.3		

Figure 10 shows that the optimal value for D is 0.16 mm, corresponding to $S_{11} = -23$ dB and $S_{21} = -0.39$ dB. The authors selected this value for the final design as it ensures superior filter performance, as demonstrated in Fig. 11.

From Fig. 11, the S_{11} were -23.5 dB, -25 dB, and -23 dB at 11 GHz, 5.98 GHz, and 5.01 GHz, respectively. The bandwidth at first center frequency 11 GHz was 338 MHz while at second center frequency 5.98 GHz was 154 MHz. The bandwidth of the third center frequency at 5.01 GHz was 38 MHz that is very narrow and more selectivity bandwidth. The S_{21} were -0.26 dB, -1 dB, and -0.39 dB at 11 GHz, 5.98 GHz, and 5.01 GHz, respectively. In this case, the return losses and insertion losses were very low in the three bands, and the signal passes at theses frequencies with small losses. To verify the responsibility of each part in the structure, the authors consider the E-filed distributions of the structure at three bands by using CST as shown in Fig. 12. The E-filed distribution at 11 GHz shown in Fig. 12(a) shows the E-filed constructed on the TLs. From this, TLs work as feeding TLs and resonators at 11 GHz. At 5.98 GHz the E-field distribution focuses at center metamaterials the 0th iteration open loop resonators; therefore, they are responsible for producing the second mode at 5.98 GHz as shown in Fig. 12(b). Finally, the E-filed distribution at 5.01 GHz, constructed from the 1st iteration Modify-Minkowski resonators, confirms that the third mode at 5.01 GHz is generated by the inclusion of these additional resonators, as shown in Fig. 12(c).

5. FABRICATION DUAL BANDS BPF

To verify the performance of the proposed triple-band bandpass filter (BPF), the design is fabricated using a ProtoMat S100, as shown in Fig. 13. Fig. 13(a) shows the top view of the filter, while Fig. 13(b) shows the bottom view, which consists of a flat copper ground plane. The proposed filter was

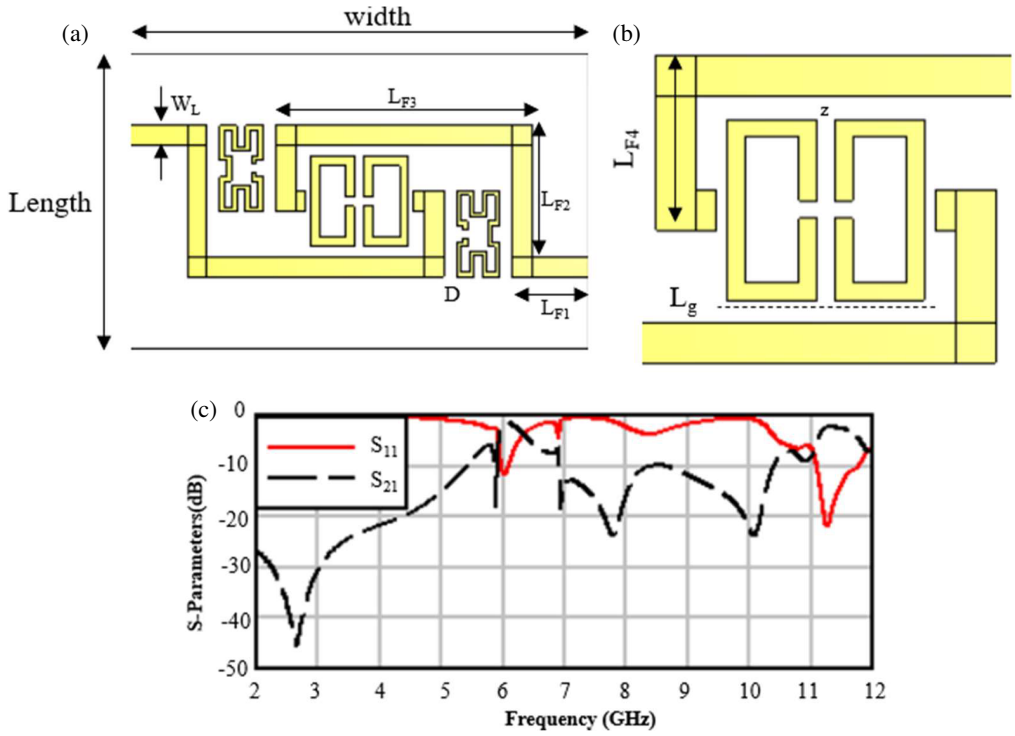

FIGURE 9. (a) The proposed triple-band BPF. (b) Zoom to the center section of the proposed BPF. (c) S-parameters of the proposed BPF.

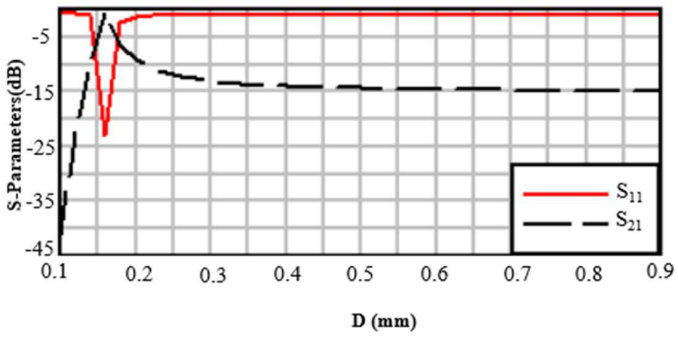

FIGURE 10. S-parameters vs D parameter.

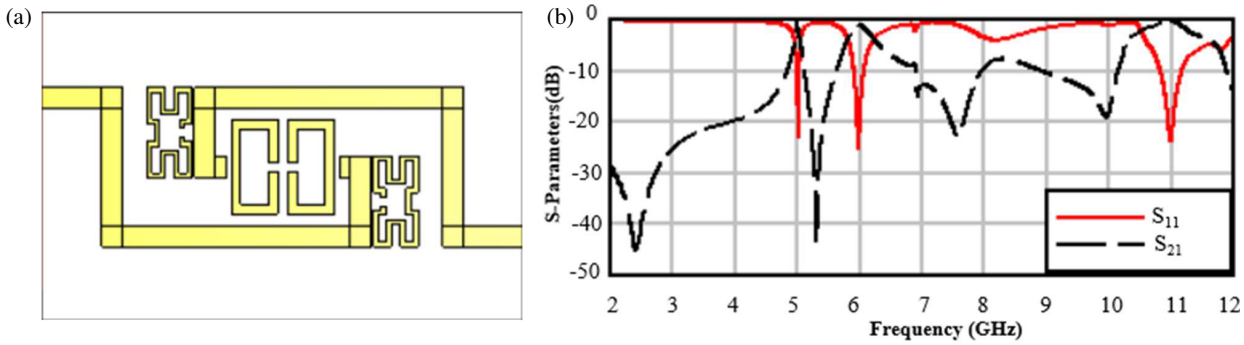

FIGURE 11. (a) The final form of the proposed triple-band BPF. (b) The S-parameters of it.

implemented on a Rogers RO4003 substrate with a thickness of 1.5 mm and a dielectric constant of 3.5. The overall dimensions of the structure are 32.2 mm × 20.6 mm. The design parameters are detailed in Table 1. Notably, distance D, which represents the distance between the first iteration resonators and the transmission lines (TLs), is 0.16 mm, contributing significantly to the performance characteristics.

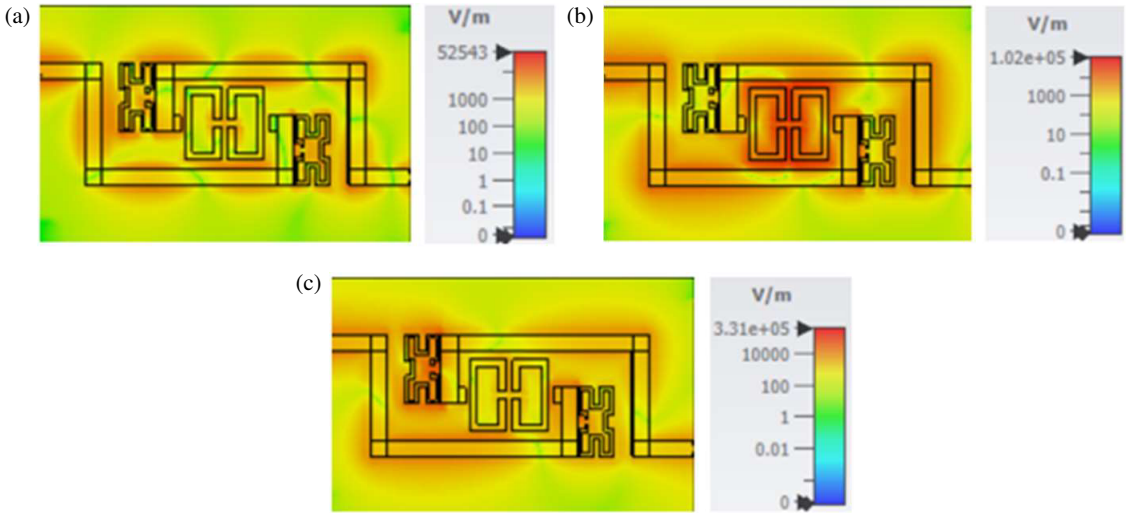

FIGURE 12. E-filed distribution at (a) 11 GHz, (b) 5.98 GHz, and (c) 5.01 GHz.

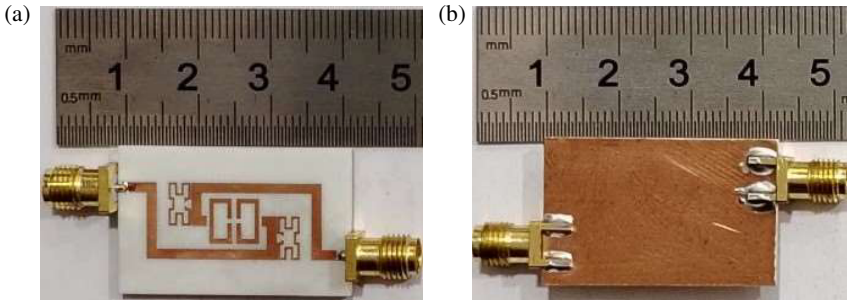

FIGURE 13. Fabrication of the proposed triple band BPF. (a) Top view. (b) Bottom view.

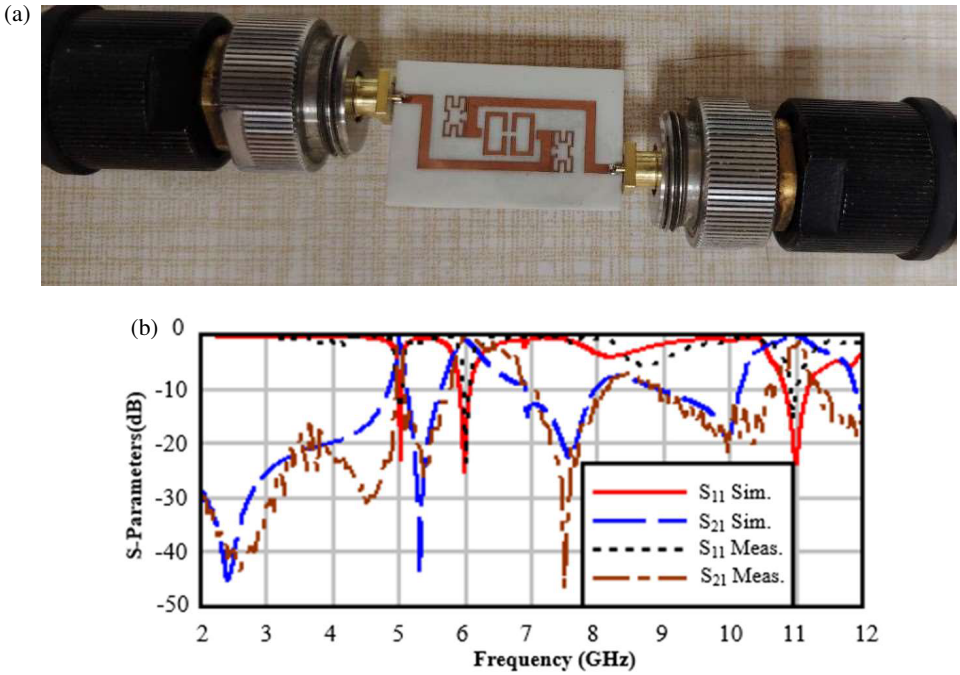

FIGURE 14. (a) The proposed triple band filter on VNA. (b) The S-parameters measurements and Simulation.

TABLE 2. Comparison between the proposed triple-band BPF and the previous works.

	Overall size $\lambda_g \times \lambda_g$	Frequency (GHz)	Insertion loss (dB)	Type	Fabrication
Reference [1]	1.02×0.65	11/6	6 /1	Dual Band	NA
Reference [2]	0.29×0.41	3.65/2.55	2.13/1.22	Dual Band	Yes
Reference [3]	0.126×0.132	5.7/2.4	0.64/0.76	Dual Band	Yes
Reference [4]	Not given	3/2/1.68	Not given	Dual Band	NA
Reference [10]	0.29×0.14	1.61	Not given	Single Band	Yes
Reference [11]	0.186×0.186	10.8/10/7.88/3.55	Not given	Quad Band	NA
Proposed work	0.85×0.54	11/6/5	0.26/1/0.39	Triple Band	Yes

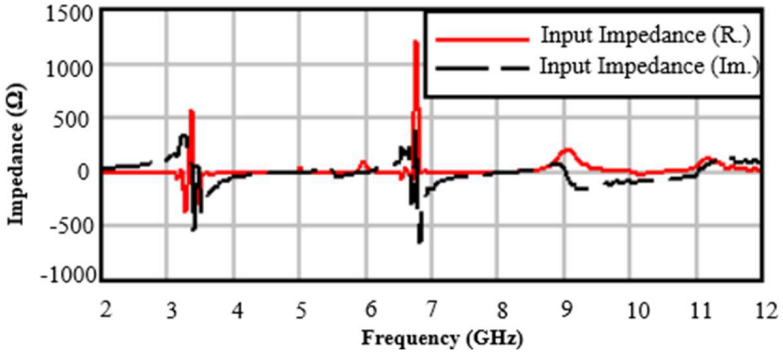

FIGURE 15. Measurements of input impedance of the proposed filter.

6. RESULTS AND MEASUREMENTS

Measurements of S-parameters and input impedance of proposed Triple BPF are implemented using Anritsu MS4642A Vector Network Analyzer (VNA). The measurement of the parameters is shown in Fig. 14 and Fig. 15. Fig. 14(b) shows a high correlation between the measurement and simulation results. Measurements of S_{11} are -15 dB, -23.3 dB, and -13 dB at 10.95 GHz, 6 GHz, and 5 GHz, respectively, while measurements of S_{21} were -1.5 dB, -0.4 dB, and -0.98 dB at 10.95 GHz, 6 GHz, and 5 GHz, respectively. The bandwidth of each band is 40 MHz at a center frequency of 10.95 GHz, 100 MHz at 6 GHz, and 60 MHz at a third center frequency of 5 GHz. The difference between measurement and simulation is because of fabrication environments, welding, and measurement accuracy.

Figure 15 shows the measured Real part (R.) and Imaginary (Im.) part of input impedance. The input impedance real parts are 52 Ω, 51 Ω, and 45.6 Ω at 10.95 GHz, 6 GHz, and 5 GHz, respectively. From this, adding 1st iteration resonators was as load to TLs that improve S_{21} as shown previously and made a good match between TLs characteristic impedance 80 Ω and port impedance 50 Ω by making the input impedance approximately equal to 50 Ω. Finally, the 1st iteration resonators have two achievements. First, they introduce a third band centered at 5 GHz. Second, they act as a load to match the input impedance to 50 Ω, ensuring good impedance matching. The authors compare the proposed work with conventional dual-band BPF of [1] in Table 2. The proposed Triple-Band BPF has lower insertion loss than previous works.

7. CONCLUSION

This paper presents a triple-band bandpass filter (BPF) incorporating metamaterials and fractal geometry. The design is structured around three main principles. Firstly, the transmission lines (TLs) serve as both feed lines and resonators at higher frequencies. Secondly, modified-Minkowski open-loop metamaterial resonators of the 0th iteration are employed for the middle frequency band. Lastly, at lower frequencies, 1st iteration modified-Minkowski resonators are introduced in the space between TLs to maximize space utilization. The filter is designed to operate at center frequencies of 11 GHz, 6 GHz, and 5 GHz, utilizing a Rogers RO4003 substrate with a thickness of 1.5 mm and a dielectric constant of 3.5. The overall dimensions of the structure are 32.2 mm $\times$ 20.6 mm. Simulations conducted using CST Microwave Studio produced S_{11} values of -23.5 dB, -25 dB, and -23 dB at 11 GHz, 5.98 GHz, and 5.01 GHz, respectively, with corresponding S_{21} values of -0.26 dB, -1 dB, and -0.39 dB. The proposed filter has a size reduction of 31%. The design is validated by fabricating a prototype of the filter, demonstrating strong agreement between the measured and simulated results. The measured input impedance is approximately 50 Ω, verifying that the 1st iteration resonators not only acted as resonators at 5 GHz but also functioned as loads to the TLs, facilitating the proper impedance matching between the TLs and input/output ports, making it a suitable choice for RF and microwave applications.

REFERENCES

[1] Berka, M., T. Islam, S. Das, A. Serhane, M. L. Kumar, and Z. Mahdjoub, "Design of miniaturized dual-band bandpass microstrip filter based on C-shaped metamaterial resonators for RF/microwave applications," *Journal of Nano-and Electronic Physics*, Vol. 16, No. 4, 04012, 2024.

[2] Ieu, W., D. Zhang, and D. Zhou, "High-selectivity dual-mode dual-band microstrip bandpass filter with multi-transmission zeros," *Electronics Letters*, Vol. 53, No. 7, 482–484, 2017.

[3] Khani, S., S. V. A.-D. Makki, S. M. H. Mousavi, M. Danaie, and P. Rezaei, "Adjustable compact dual-band microstrip bandpass filter using T-shaped resonators," *Microwave and Optical Technology Letters*, Vol. 59, No. 12, 2970–2975, 2017.

[4] Hammas, H. A., "Design of compact multiband microstrip BPF based on fractal open-ring configuration," *Engineering and Technology Journal*, Vol. 36, No. 8, Part A, 887–890, 2018.

[5] Ahmed, H. S., A. J. Salim, and J. K. Ali, "A compact dual-band bandstop filter based on fractal microstrip resonators," in *Progress In Electromagnetics Research Symposium, PIERS*, Prague, Czech Republic, Jul. 2015.

[6] Ahmed, H. S., J. K. Ali, A. J. Salim, and N. N. Hussain, "A compact triple band BSF design based on Minkowski fractal Geometry," in *2016 18th Mediterranean Electrotechnical Conference (MELECON)*, 1–5, Lemesos, Cyprus, Apr. 2016.

[7] Chakraborty, U., A. Kundu, S. K. Chowdhury, and A. K. Bhattacharjee, "Compact dual-band microstrip antenna for IEEE 802.11 a WLAN application," *IEEE Antennas and Wireless Propagation Letters*, Vol. 13, 407–410, 2014.

[8] Küçükcan, S. and A. Kaya, "Dual-band microstrip patch antenna design for Wi-Fi applications," *Avrupa Bilim ve Teknoloji Dergisi*, No. 34, 661–664, 2022.

[9] Ali, I. and R. Y. Chang, "Design of dual-band microstrip patch antenna with defected ground plane for modern wireless applications," in *2015 IEEE 82nd Vehicular Technology Conference (VTC2015-Fall)*, 1–5, Boston, MA, USA, Sep. 2015.

[10] Ali, J. K. and H. T. Ziboon, "Design of compact bandpass filters based on fractal defected ground structure (DGS) resonators," *Indian Journal of Science and Technology*, Vol. 9, No. 39, 1–9, 2016.

[11] Ziboon, H. T. and J. K. Ali, "Compact quad-band BPF design with fractal stepped-impedance ring resonator," *ARPN Journal of Engineering and Applied Sciences*, Vol. 12, No. 24, 7352–7363, 2017.

[12] Ahmed, H. S., A. J. Salim, M. R. Hussan, H. A. Hammas, M. T. Yassen, S. Mutashar, and J. K. Ali, "Design of compact dual-mode fractal based microstrip band reject filter," *ARPN Journal of Engineering and Applied Sciences*, Vol. 13, No. 7, 2395–2399, 2018.

[13] Ahmed, H. S., A. J. Salim, J. K. Ali, and M. A. Alqaisy, "A fractal-based dual-mode microstrip bandstop filter for wireless applications," in *2016 16th Mediterranean Microwave Symposium (MMS)*, 1–4, Abu Dhabi, United Arab Emirates, Nov. 2016.

[14] Qing, X. M., Y. W. M. Chia, and J. Sun, "A novel miniaturized microstrip bandpass filter using a meander-line resonator," *Microwave and Optical Technology Letters*, Vol. 32, No. 4, 319–321, 2002.

[15] Su, G. Y., C. N. Chan, U. L. Tam, and K. W. Tam, "Compact microstrip lowpass filter using a meander-line structure," *Microwave and Optical Technology Letters*, Vol. 48, No. 7, 1339–1341, 2006.

[16] Ahmed, H. S., *Microwave Ovens Leakage Reduction Using Band-Reject Filter: Applying the Fractal Band-Reject Filter*, LAP Lambert Academic Publishing, 2017.

[17] Pozar, D. M., *Microwave engineering*, Fourth Editions, University of Massachusetts at Amherst, John Wiley & Sons, Inc, 2012.

[18] Thomann, W., B. Isele, and P. Russer, "Characterization of a 90 degrees curved microstrip transmission line in the time-domain and frequency-domain with 3D-TLM-method and measurements," in *IEEE Antennas and Propagation Society International Symposium 1992 Digest*, 658–661, Chicago, IL, USA, Jun. 1992.

[19] Nicolson, A. M. and G. F. Ross, "Measurement of the intrinsic properties of materials by time-domain techniques," *IEEE Transactions on Instrumentation and Measurement*, Vol. 19, No. 4, 377–382, 1970.

[20] Weir, W. B., "Automatic measurement of complex dielectric constant and permeability at microwave frequencies," *Proceedings of the IEEE*, Vol. 62, No. 1, 33–36, 1974.

[21] Sharma, S. and R. Mehra, "Printed monopole slot antenna inspired by metamaterial unit cell for wireless applications," in *Optical and Wireless Technologies: Proceedings of OWT 2020*, 413–424, 2022.